Hyperbolic Polaritonic Crystals Based on Nanostructured Nanorod Metamaterials

Dickson, W., Beckett, S., McClatchey, C., Murphy, A., O'Connor, D., Wurtz, G. A., Pollard, R., & Zayats, A. V. (2015). Hyperbolic Polaritonic Crystals Based on Nanostructured Nanorod Metamaterials. *Advanced materials (Deerfield Beach, Fla.)*, *27*(39), 5974-80. https://doi.org/10.1002/adma.201501325

Published in:
Advanced materials (Deerfield Beach, Fla.)

Document Version:
Publisher's PDF, also known as Version of record

ADVANCED MATERIALS
www.advmat.de

www.MaterialsViews.com

Hyperbolic Polaritonic Crystals Based on Nanostructured Nanorod Metamaterials

Wayne Dickson, Stephen Beckett, Christina McClatchey, Antony Murphy, Daniel O'Connor, Gregory A. Wurtz, Robert Pollard, and Anatoly V. Zayats*

The optical properties of metallic nanoparticles, films, and surfaces are determined by surface plasmon excitations[1] and provide the framework for the manipulation of light on the nanoscale,[2,3] including generation, absorption, confinement, and guiding.[4,5] Physical limitations imposed by the permittivity of the metal restrict the dispersive properties of surface plasmon polaritons (SPPs) and thus the design of SPP-based components, mostly compounded by the narrow choice of metals with useful plasmonic properties throughout the visible and near infrared spectral range. While significant effort is currently devoted to the development of novel plasmonic materials,[6,7] the structuring of conventional plasmonic metals also provides a route to control plasmonic waves. Periodically nanostructured metallic films, termed plasmonic crystals, facilitate coupling between photons and SPPs and demonstrate unique and controllable optical properties determined by a combination of design geometry (period and elementary cell), the surrounding dielectric permittivity, and the choice of metal.[8,9] As a result, the optical resonances of plasmonic crystals, exhibiting strong electromagnetic field enhancement, are possible at frequencies ranging from the ultraviolet to the near infrared,[7,10] an approach which may be extended to even lower frequencies by utilizing so-called spoof plasmons.[11]

In the same context, the development of anisotropic optical metamaterials,[12–16] exhibiting hyperbolic dispersion, provides the ability to achieve significant control over the effective permittivity and has already led to the design of many new functionalities including subwavelength imaging,[14,15,17] increased spontaneous emission,[18,19] high-performance sensing,[20,21] and enhanced non-linearities.[22] Self-assembled arrays of gold nanorods have recently attracted significant interest as modular optical metamaterials, mainly as a result of their ease of fabrication and inherent optical anisotropy, presenting the opportunity to tailor the frequency onset of hyperbolic dispersion throughout the visible and infrared spectral range.[16,23]

In this paper, we combine the functionality provided by metamaterials and photonic-crystal-type structures to demonstrate metamaterial-based photonic crystals, termed hyperbolic polaritonic crystals (HPCs). By employing a fully flexible plasmonic nanorod metamaterial platform exhibiting hyperbolic dispersion and tunable epsilon-near-zero (ENZ) frequency[15,24] determining the plasmonic behavior of the metamaterial similar to the plasma frequency for bulk metals,[25] we show how both the resonant response of HPCs and their mode confinement capability can be controlled. The unique approach described here provides the opportunity to tailor the HPC's optical response both extrinsically, through nanostructuring, and intrinsically through the metamaterial's effective permittivity design, including its hyperbolic dispersion, by dimensional nanorod array parameterization. As a result, HPCs comprised mainly of dielectric patches separated by metamaterial areas only a few nanorods across, provide a flexible alternative to conventional plasmonic metals in applications requiring on-demand engineering of plasmonic behavior. They may also be used for light coupling to, and extraction from, waveguided modes of hyperbolic metamaterials, inaccessible via conventional or total-internal reflection illumination due to their very high modal effective index, but which play a significant role in conditioning both the non-linear response of hyperbolic metamaterials and their spontaneous emission properties.

We consider metamaterials composed of plasmonic nanorod arrays (**Figure 1**a) fabricated in self-assembled anodic aluminum oxide (AAO) templates (see Methods in the Supporting Information). The typical extinction spectrum of the metamaterial under plane wave illumination shows two resonances linked to the plasmonic response of the metamaterial for the electromagnetic field polarized along either short or long nanorod axis (Figure 1a).[24] These optical properties result from the anisotropy of the metamaterial, which can be described using effective medium theory (EMT) by the effective permittivity tensor $\varepsilon_{xx}(\omega) = \varepsilon_{yy}(\omega) \neq \varepsilon_{zz}(\omega)$ (see the Supporting Information for details). The spectral dispersion of the permittivity tensor results from the coupling between the plasmonic resonances of the individual nanorods in the array. Hyperbolic dispersion, where ε_{xx}, $\varepsilon_{yy} > 0$ and $\varepsilon_{zz} < 0$, is observed for frequencies lower than the effective plasma frequency (where $\mathrm{Re}(\varepsilon_{zz}) = 0$) of the metamaterial (Figure 1b). In this regime, the metamaterial has

Dr. W. Dickson, Dr. G. A. Wurtz, Prof. A. V. Zayats
Department of Physics
King's College London
Strand, London WC2R 2LS, UK
E-mail: wayne.dickson@kcl.ac.uk
Dr. S. Beckett, Dr. C. McClatchey, Dr. A. Murphy, Dr. R. Pollard
Centre for Nanostructured Media
The Queen's University of Belfast
Belfast BT7 1NN, UK
Dr. D. O'Connor
National Physical Laboratory
Teddington TW11 0LW, UK

DOI: 10.1002/adma.201501325

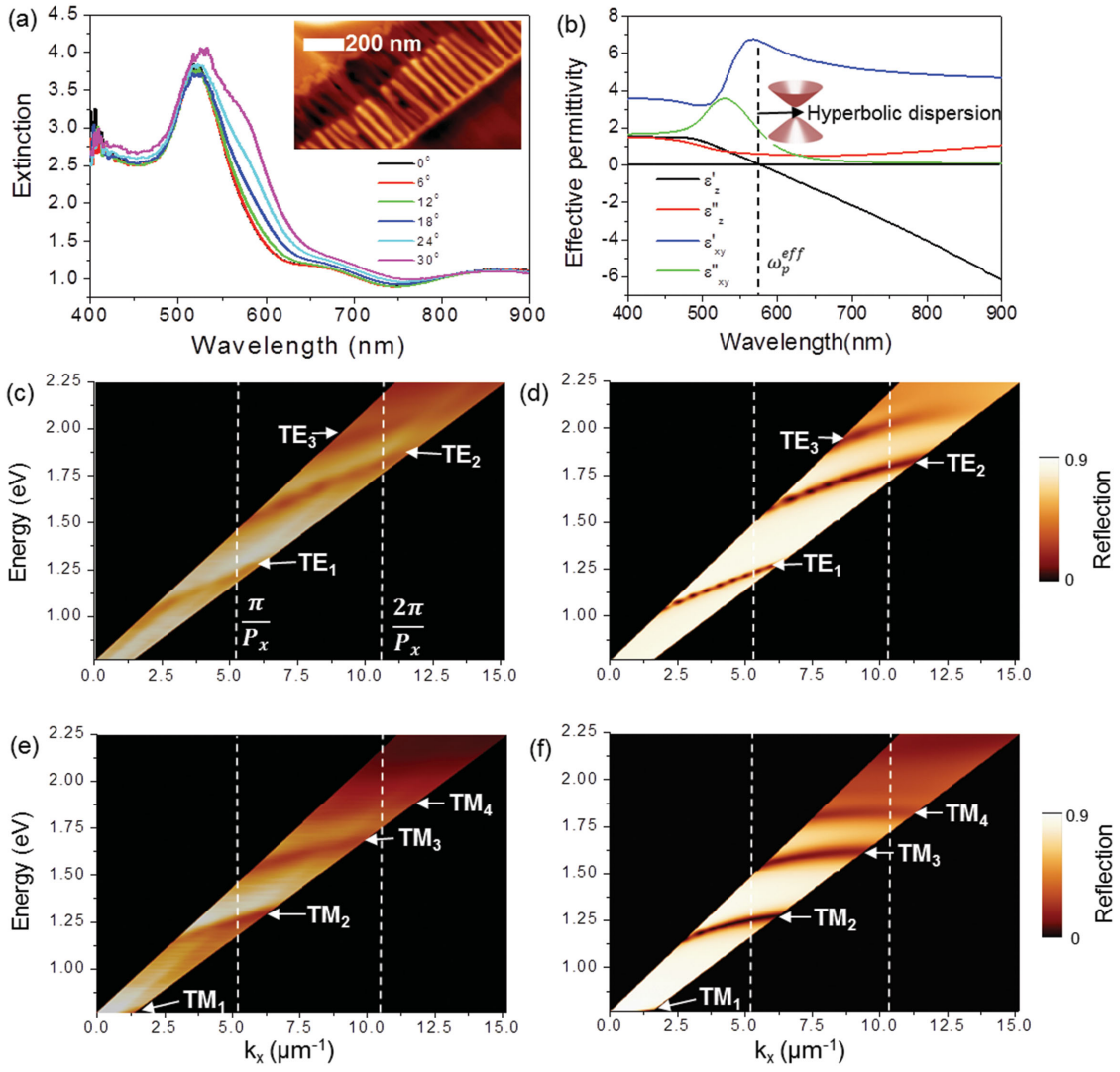

Figure 1. Structural and optical properties of the Au nanorod metamaterial. a) Extinction spectra at different incident angles of the unstructured metamaterial (inset: cross-section showing metamaterial structure. b) Effective permittivity of the metamaterial; the effective plasma frequency and elliptical to hyperbolic dispersion ranges are indicated. c–f) Reflectivity dispersion of the unstructured metamaterial slab for (c), (d) TE and (e), (f) TM polarisations: (c), (e) experiment and (d), (f) numerical simulations. The dashed white lines indicate the positions of the first and second Brillouin zones in the Γ-X direction for a HPC having a period P_x = 700 nm.

plasmonic properties for extraordinary waves, i.e., waves with an electric field polarized along the nanorod axes. It should be noted that nonlocal effects, which can be observed in nanorod based metamaterials,[26,27] were not observed experimentally or numerically in the metamaterial considered, where the bulk-plasma frequency is close to the Au interband absorption and local EMT was therefore applied throughout.

The attenuated total reflection (ATR) spectra of the metamaterial slab exhibit features clearly illustrating the existence of guided modes, manifested as minima in the reflection spectrum for both transverse electric (TE) and transverse magnetic (TM) polarizations (Figure 1c,e). In the asymmetric surroundings of the metamaterial slab, these waveguided modes become leaky between light lines in the superstrate (air) and the substrate (glass), making them accessible to free-space radiation from the substrate, and thus to ATR measurements. These modes extend throughout the studied spectral range with a high-frequency cut-off determined by the position of the effective plasma frequency $\omega_p^{eff} \approx 2.17$ eV of the metamaterial[25] (Figure 1b). For frequencies below ω_p^{eff}, TM modes are hyperbolic waveguided modes (HWMs), resulting from the 1D confinement of hyperbolic plasmon-polaritons supported by the unbounded metamaterial. Both phase and group velocities, as well as group velocity dispersion (GVD) of HWMs are determined by the geometry of the metamaterial, such as nanorod diameter, length, separation, as well as the permittivities of both the metal and embedding medium. TE modes have a greater group velocity than TM modes due to the different effective permittivity of the metamaterial seen by these modes (Figure 1c,e). Numerical calculations of the metamaterial's optical properties employing EMT demonstrate excellent agreement with experimental measurements (Figure 1c–f). The

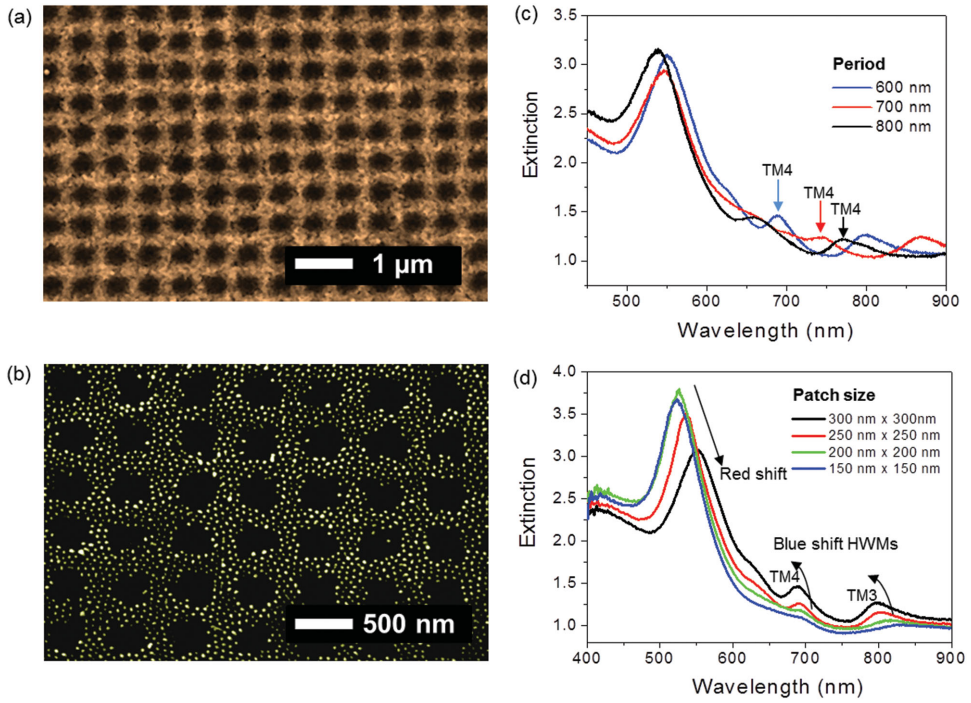

Figure 2. Structural and optical properties of the hyperbolic polaritonic crystals. a) Scanning electron microscopy (SEM) image of the alumina template after periodic patterning: (dark areas) regions of closed pores in the template. b) SEM image of the periodically structured nanorod metamaterial after removal of alumina template: (dark areas) air, (bright features) individual Au nanorods; only 3–4 nanorods separate the dielectric patches. c,d) Normal incidence extinction spectra of the HPC for (c) different periods (dielectric patch size is 300 nm) and (d) different dielectric patch sizes (period is 600 nm); the incident light polarization is aligned with the axis of the square periodic lattice. In (c) and (d) the position of the modes are indicated as a guide to the eye.

metamaterial geometry and boundary conditions determine the structure of the supported modes, which have been identified from both the numerically calculated electromagnetic field distributions (Figure S3, Supporting Information) and analytical theory (see Methods in the Supporting Information).

In order to form the HPC, the metamaterial slab is periodically structured in a square lattice with periodicities ranging from 600 to 800 nm (**Figure 2**a,b) using a procedure described in the Methods in the Supporting Information. This results in the metamaterial being periodically punctured with dielectric patches ranging from 150 nm × 150 nm to 300 nm × 300 nm in size (Figure 2b). The dielectric patches are separated by metamaterial areas comprised of only 3–4 nanorods for a period of 600 nm (300 nm square dielectric patch) and 8–9 nanorods for a 800 nm period structure (150 nm square dielectric patch). The periodic structuring of the metamaterial generates a family of Bragg-scattered waveguided modes leading to the formation of hyperbolic waveguided Bloch modes, in analogy to the modes of 2D dielectric photonic crystals or plasmonic crystals, where the periodic structuring of a continuous metallic film with a period comparable to the SPP wavelength leads to the formation of SPP Bloch modes on the nanostructured interface.[8] The periodic structuring ensures momentum matching to couple free-space radiation to the metamaterial Bloch modes as well as coupling to HWMs of the surrounding unstructured metamaterial, in analogy to grating couplers for plasmonic or dielectric waveguides.

In comparison to the unstructured metamaterial, the extinction spectra of HPCs reveal additional resonances in the region of hyperbolic dispersion, having spectral locations dependent on the period of the structure (Figure 2c). This is consistent with the folding of the modes in the Brillouin zones of the fabricated 2D crystal lattice (Figure 1c–e). One can see the striking difference between TE and TM Bloch modes related to the difference in the dispersion of the TE and TM modes: TE modes, before folding, have positive dispersion while TM modes show negative dispersion at high wavevectors (Figure 1 and Figure S4 and S5, Supporting Information). The mode folding due to the periodic structure brings the region of negative dispersion within the light cone, allowing access to these unusual modes under conventional illumination of the HPC, modes which would not be accessible in the unstructured metamaterial. Despite the small number of constituent nanorods between adjacent dielectric patches comprising the metamaterial, hyperbolic waveguided modes are still observed. For small dielectric patches (150 nm × 150 nm, corresponding to the removal of approximately four nanorods), the low scattering cross-section of the patches reduces the Bragg efficiency of the HPC (Figure 2d). As the size of the patch, determining the lattice basis, is increased, a small but distinct blue-shift of the resonance wavelengths is observed (Figure 2d), similar to the blue-shift the SPP band gap edge of the plasmonic crystal with the increasing hole size.[28]

Due to the reduced number of nanorods (3–4 nanorods) forming the metamaterial area between dielectric patches, the

effective permittivity of the metamaterial in the structured area no longer precisely corresponds to the effective permittivity of the metamaterial before structuring. This is due to a modification in the inter-rod electromagnetic coupling depending on local environment, which is different in areas with fewer interacting nanorods. As a result, it is apparent that as dielectric patch size increases, so does the coupling efficiency of the incident free-space photons to the hyperbolic waveguided Bloch modes supported by the HPC, as evidenced by the increased extinction at the resonant frequencies, and is here related to an increase in the scattering cross-section of the dielectric patches compared to the surrounding media. The ability to couple to these modes via conventional illumination, and in particular at normal incidence, opens up new opportunities to couple free-space radiation to high index, highly confined modes, inaccessible through conventional prism coupling and critical for slow light applications and the control of spontaneous emission. Additionally, the introduction of periodic nanostructuring affects the modes both by introducing spectral broadening, resulting from Bragg-induced radiation losses and spectral mode dispersion, due to modified inter-rod interactions (**Figure 3**). As the in-plane wavevector of the modes increases, their folding at the Brillouin zone edges leads to an observable splitting for TE polarized modes only. For TM modes, the counter-propagating diffracted orders (±1,0) cannot be resolved due to a much lower group velocity of the modes in the range of mode indices probed here. It was theoretically shown that in 1D hyper-crystals formed by natural materials with hyperbolic dispersion Dirac-type dispersion can also be observed.[29]

The unstructured nanorod metamaterial layer supports a variety of TM modes (Figure 1). When compared to the dispersion of SPPs at a smooth metal–air interface, it is clear that the metamaterial provides extensive flexibility in the design of modal effective index, as illustrated in Figure S5 (Supporting Information), where extending the effective medium approach to examine the modal behavior beyond the experimentally measurable range of wavevectors recovers the experimental observations made in Figure 1c,e for wavevectors corresponding to leaky modes, present between the light lines in the substrate and superstrate. However, the modes of the metamaterial slab exhibit negative group velocity when the modal index is either greater than that of the substrate (fully guided regime) or smaller than that of the superstrate (unbounded modes), in which case, the metamaterial slab essentially acts as a low Q-factor Fabry–Perot resonator. The characteristic electromagnetic field distributions for both TE and TM modes are shown in **Figure 4**c–f and Figure S3c–f (Supporting Information) and agree with conventional waveguiding theory.[30]

To illustrate the flexibility of the system for light guiding at a particular wavelength, the full complex modal index has been calculated using eigenmode analysis for weakly ($n_{\text{eff}} < 1.5$) and strongly ($n_{\text{eff}} > 1.5$) confined modes, highlighting the ability to choose the desired modal index within a narrow spectral bandwidth. The unstructured nanorod metamaterial layer supports a variety of TM modes with in-plane momentum which can be well-approximated within the effective medium theory as:[25]

$$\beta_{\text{TM}}(\omega) = \sqrt{\varepsilon_{zz}^{\text{eff}}(\omega/c)^2 - \varepsilon_{zz}^{\text{eff}}/\varepsilon_{xx}^{\text{eff}}(q\pi/L)^2} \quad (1)$$

where permittivities are assumed frequency-dependent, q is a nonzero positive integer referring to the mode order, and L is the thickness of the metamaterial layer, leading to an effective index for each mode q expressed as:

$$n_q^{\text{eff\_TM}} = n_{zz}^{\text{eff}}\sqrt{1-(q\pi c/n_{xx}^{\text{eff}}L\omega)^2} \quad (2)$$

where $n_{xx,zz}^{\text{eff}} = \sqrt{\varepsilon_{xx,zz}^{\text{eff}}}$. When compared to the dispersion of SPPs at a smooth metal–air interface, it is clear that the metamaterial provides extensive flexibility in the design of the modal effective index with the ability to achieve similar effective index

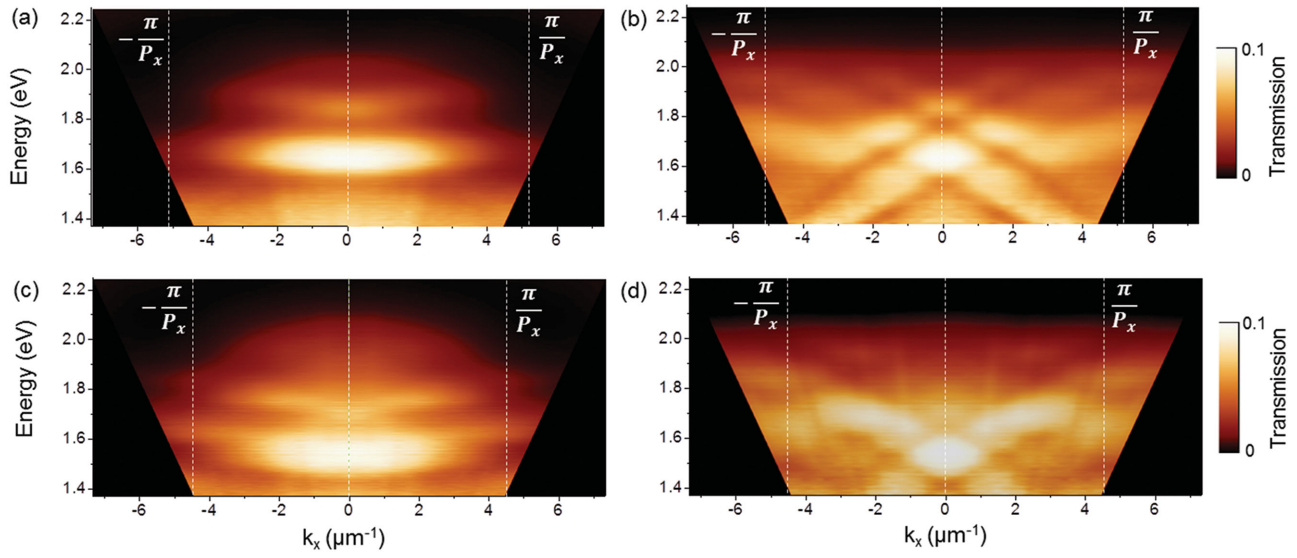

Figure 3. Transmission dispersion of hyperbolic polaritonic crystal. Angular dependent transmission spectra for a,c) TM and b,d) TE polarizations of the incident light for the HPC with a period, P_x, of 600 nm (a,b) and 700 nm (c,d). In both cases the dielectric patch size is 300 nm (three rods between the adjacent patches). The positions of the first Brillouin zone of the HPCs in the Γ-X direction are marked with dashed white lines.

ADVANCED MATERIALS
www.advmat.de

www.MaterialsViews.com

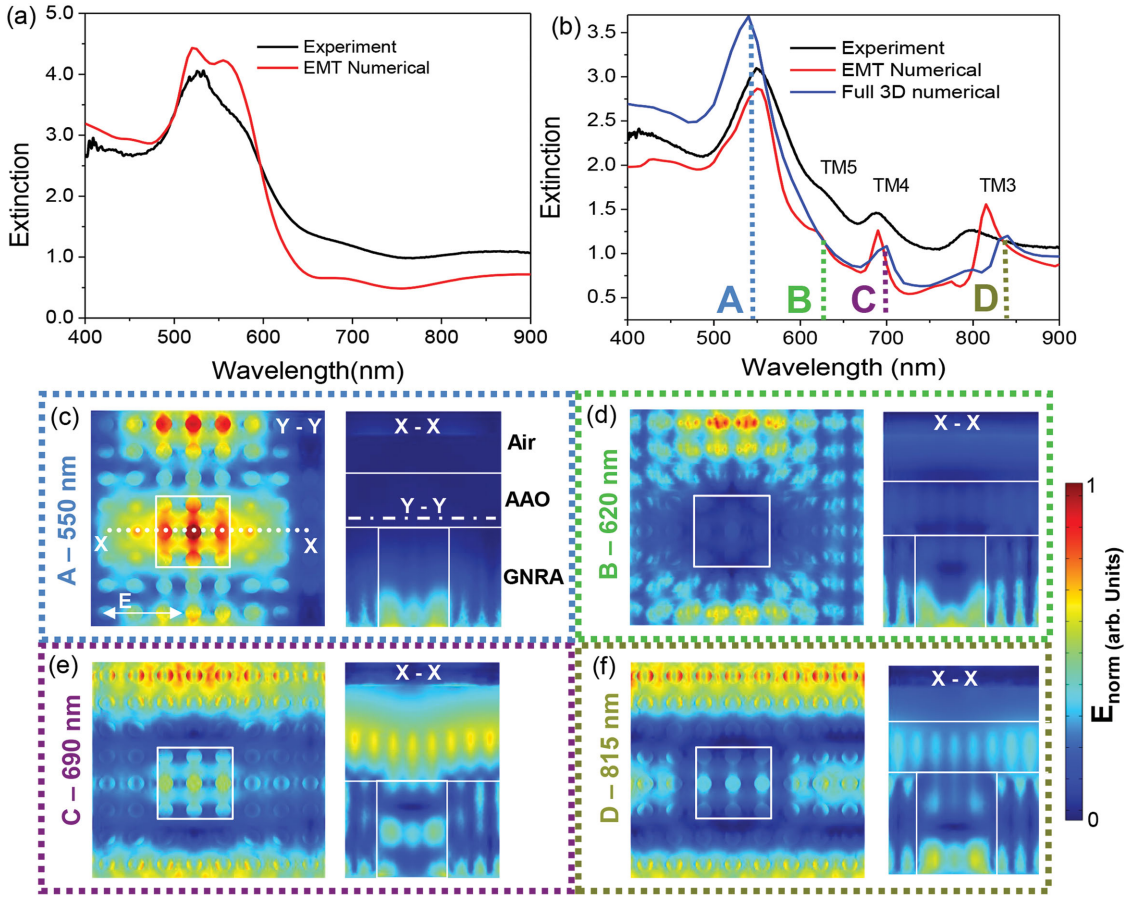

Figure 4. Electromagnetic field distribution in a HPC. Experimental and simulated extinction spectra for a) unstructured metamaterial at an angle of incidence of 30° (TM-polarised light) and b) HPC (period 600 nm, dielectric patch 300 nm, three nanorods between the patches) at normal incidence. c–f) Electric field distributions (norm of the electric field **E**) at positions A–D identified in (b) showing both a plan view (*Y*–*Y*) taken 10 nm above the HPC and horizontal cross-section (*X*–*X*) through the center of the metamaterial layer. The direction of the cross-section and incident light polarization are shown in (c) and are the same for all images.

simultaneously at multiple frequencies as well as narrowband multimodal behavior. For the geometry considered here, effective indices exceeding $\mathrm{Re}(n_q^{\mathrm{eff\_TM}}) = 5$ can be achieved simultaneously at multiple frequencies, dictated by the mode order q, throughout both visible and infrared spectral ranges. HWMs show strong field confinement within the metamaterial layer, a property that scales with $n_q^{\mathrm{eff\_TM}}$ and that is largely preserved after Bloch mode formation as attested in both the far-field measurements, where HWMs correspond to minima/maxima in reflectance/extinction, and more directly in the calculated near-field maps (Figure 4 and Figure S3, S5, and S6, Supporting Information). The penetration depth of TM electromagnetic modes on a flat interface between the nanorod metamaterial and a medium of refractive index n can be expressed as:

$$\delta_q = (2k_0\sqrt{|n^2 - (\mathrm{Re}(n_q^{\mathrm{eff\_TM}}))^2|})^{-1} \quad (3)$$

Similarly, for SPP modes on a flat Au/dielectric interface, this corresponds to:

$$\delta_d = (2k_0\sqrt{n/(|\mathrm{Re}(\varepsilon_m)| + \sqrt{n})})^{-1} \quad (4)$$

For a free space wavelength of 1.5 µm, these values are ≈1.25 µm for an SPP at an Au/air interface and ≈50 nm for the HPC TM fundamental mode $q = 1$ with $n_1^{\mathrm{eff\_TM}} \approx 2.9$ for a metamaterial thickness of 400 nm. Thus, HPC modes provide more than 20 times stronger confinement. For the $q = 1$ TE mode in the metamaterial, the effective refractive index is much lower $n_1^{\mathrm{eff\_TE}} \approx 1.6$ with a penetration depth of about 100 nm. Despite the small quantity of metal present in the HPC (dielectric patches are separated by the metamaterial areas of only a few plasmonic nanorods across), the waveguided modes of these structures at telecom wavelengths have confinement ten times superior to conventional surface plasmon polaritons on a smooth Au/air interface. In the case of SPPs on a metallic film, such high mode indices are difficult to achieve due to loss-induced back bending of the SPP dispersion,[10] notwithstanding the flexibility afforded by the metamaterial system here, in choosing the wavelength of operation and mode order with unprecedented flexibility.

Numerical simulations confirm the HPC Bloch mode formation and the observed optical properties of structured metamaterials (Figure 4 and Figure S6, Supporting Information). Despite the inference that periodic structuring of the nanorod

array perturbs the effective index of the metamaterial, this effect only results in a small additional frequency shift of the features in the extinction spectra, and both the EMT approach and the full 3D simulations demonstrate excellent qualitative and quantitative agreement with each other, and with the resonances associated with the Bloch modes measured experimentally. The simulated electric field distributions near the extinction peak in the elliptic regime (position A) and HWMs (positions B–D) are shown in Figure 4a–d and Figure S6 (Supporting Information). The electromagnetic field distributions of the HWMs exhibit the expected Bloch mode structure and confirm the waveguided origin of the modes within the structured layer, encompassing modes TM3–TM5 in direct analogy with the field distributions for the unstructured area (Figure S3, Supporting Information). These modes exhibit a typical Fabry–Perot like structure verifying that Bragg coupling to waveguided modes has indeed been achieved by periodic nanostructuring. The electromagnetic field distributions, calculated for the periodically nanostructured area using both the full 3D (Figure 4c) and effective medium approach (Figure S6c, Supporting Information), are in close agreement with differences arising from field confinement effects due to either the presence of nanorods or empty pores in the AAO matrix.[31] As can be observed on examination of Figure 4c–f, the full 3D simulation reveals regions of high field confinement with a length scale on the order of the rod diameter (≈ 40 nm), in both the metamaterial and the dielectric patches.

In conclusion, we have fabricated hyperbolic polaritonic crystals via wavelength-scale structuring of plasmonic nanorod-based hyperbolic metamaterials. We have experimentally demonstrated the formation of a designed Bloch-mode band-structure of hyperbolic guided waves and the inherent coupling of free-space radiation to high-index modes of the metamaterial. Strikingly, despite being comprised of areas of only a few (as few as 3) nanorods across, the metamaterial behavior of the hyperbolic polaritonic crystals is preserved. These hyperbolic Bloch modes have several significant advantages over either modes of dielectric waveguides or surface plasmon polaritons modes; they provide strong confinement in deep-subwavelength waveguides with the modal indices reaching 5, not achievable in dielectrics, and provide flexible design of the dispersion via metamaterial properties, which would be otherwise fixed by the plasmonic metal properties. Several distinct modes exist throughout the visible and infrared region of the electromagnetic spectrum providing multiplexing capabilities within nanoscale optical components. In particular, this approach benefits from the combined tunability afforded by the dual design freedom of the metamaterial's optical dispersion from both the bottom-up (nanorod parameters, thickness) and by top-down nanostructuring. Moreover, the high refractive index sensitivity exhibited by the waveguided modes in the nanorod metamaterial[20] may be advantageously exploited in designer nanostructures. Nanoscale non-linear optical devices may be created either with bare nanorods[22] or when hybridized with active media,[24] and these materials also present an ideal opportunity to develop highly integrated, multiwavelength lab-on-a-chip devices with enhanced sensing capabilities. Both of these applications can be further enhanced by the ability to employ sub-attolitre controlled core–shell geometry.[32] Such highly tunable metamaterials represent a new class of plasmonic platform with enormous potential in future active and passive nanophotonic applications.

Supporting Information

Supporting Information is available from the Wiley Online Library or from the author.

Acknowledgements

This work was supported, in part, by EPSRC (UK) and the ERC iPLASMM project (321268). A.V.Z. acknowledges support from the Royal Society and the Wolfson Foundation. G.A.W. acknowledges support from the EC FP7 project 304179 (Marie Curie Actions).

Received: March 19, 2015
Revised: May 26, 2015
Published online: August 28, 2015

[1] A. V. Zayats, S. Maier, *Active Plasmonics and Tuneable Plasmonic Metamaterials*, John Wiley & Sons, Hoboken, NJ, USA **2013**.
[2] M. L. Brongersma, V. M. Shalaev, *Science* **2010**, *328*, 440.
[3] E. Ozbay, *Science* **2006**, *311*, 189.
[4] D. K. Gramotnev, S. I. Bozhevolnyi, *Nat. Photonics* **2010**, *4*, 83.
[5] A. V. Zayats, I. I. Smolyaninov, A. A. Maradudin, *Phys. Rep.* **2005**, *408*, 131.
[6] B. Luk'yanchuk, N. I. Zheludev, S. A. Maier, N. J. Halas, P. Nordlander, H. Giessen, C. T. Chong, *Nat. Mater.* **2010**, *9*, 707.
[7] P. R. West, S. Ishii, G. V. Naik, N. K. Emani, V. M. Shalaev, A. Boltasseva, *Laser Photonics Rev.* **2010**, *4*, 795.
[8] J.-S. Bouillard, S. Vilain, W. Dickson, A. Zayats, *Opt. Express* **2010**, *18*, 16513.
[9] W. Dickson, G. A. Wurtz, P. R. Evans, R. J. Pollard, A. V. Zayats, *Nano Lett.* **2008**, *8*, 281.
[10] S. A. Maier, *Plasmonics: Fundamentals and Applications: Fundamentals and Applications*, Springer, New York **2007**.
[11] J. Pendry, L. Martin-Moreno, F. Garcia-Vidal, *Science* **2004**, *305*, 847.
[12] A. Poddubny, I. Iorsh, P. Belov, Y. Kivshar, *Nat. Photonics* **2013**, *7*, 948.
[13] W. D. Newman, C. L. Cortes, Z. Jacob, *J. Opt. Soc. Am. B* **2013**, *30*, 766.
[14] C. García-Meca, J. Hurtado, J. Martí, A. Martínez, W. Dickson, A. V. Zayats, *Phys. Rev. Lett.* **2011**, *106*, 067402.
[15] R. Wangberg, J. Elser, E. E. Narimanov, V. A. Podolskiy, *J. Opt. Soc. Am. B* **2006**, *23*, 498.
[16] R. Atkinson, W. Hendren, G. Wurtz, W. Dickson, A. Zayats, P. Evans, R. Pollard, *Phys. Rev. B* **2006**, *73*, 235402.
[17] Z. Liu, H. Lee, Y. Xiong, C. Sun, X. Zhang, *Science* **2007**, *315*, 1686.
[18] S. M. Prokes, O. J. Glembocki, J. E. Livenere, T. U. Tumkur, J. K. Kitur, G. Zhu, B. Wells, V. A. Podolskiy, M. A. Noginov, *Opt. Express* **2013**, *21*, 14962.
[19] A. N. Poddubny, P. A. Belov, P. Ginzburg, A. V. Zayats, Y. S. Kivshar, *Phys. Rev. B* **2012**, *86*, 035148.
[20] A. V. Kabashin, P. Evans, S. Pastkovsky, W. Hendren, G. Wurtz, R. Atkinson, R. Pollard, V. Podolskiy, A. Zayats, *Nat. Mater.* **2009**, *8*, 867.
[21] V. V. Yakovlev, W. Dickson, A. Murphy, J. McPhillips, R. J. Pollard, V. A. Podolskiy, A. V. Zayats, *Adv. Mater.* **2013**, *25*, 2351.
[22] G. A. Wurtz, R. Pollard, W. Hendren, G. Wiederrecht, D. Gosztola, V. A. Podolskiy, A. V. Zayats, *Nat. Nanotechnol.* **2011**, *6*, 107.
[23] P. Evans, W. R. Hendren, R. Atkinson, G. A. Wurtz, W. Dickson, A. V. Zayats, R. J. Pollard, *Nanotechnology* **2006**, *17*, 5746.

[24] W. Dickson, G. Wurtz, P. Evans, D. O'Connor, R. Atkinson, R. Pollard, A. Zayats, *Phys. Rev. B* **2007**, *76*, 115411.
[25] N. Vasilantonakis, M. E. Nasir, W. Dickson, G. A. Wurtz, A. V. Zayats, *Laser Photonics Rev.* **2015**, *9*, 345.
[26] R. Pollard, A. Murphy, W. Hendren, P. Evans, R. Atkinson, G. Wurtz, A. Zayats, V. Podolskiy, *Phys. Rev. Lett.* **2009**, *102*, 127405.
[27] B. M. Wells, A. V. Zayats, V. A. Podolskiy, *Phys. Rev. B* **2014**, *89*, 035111.
[28] K. L. van der Molen, F. B. Segerink, N. F. van Hulst, L. Kuipers, *Appl. Phys. Lett.* **2004**, *85*, 4316.
[29] E. Narimanov, *Faraday Discuss.* **2014**, *178*, 45.
[30] J. D. Jackson, J. D. Jackson, *Classical Electrodynamics*, Wiley, New York **1962**.
[31] K.-T. Tsai, G. A. Wurtz, J.-Y. Chu, T.-Y. Cheng, H.-H. Wang, A. V. Krasavin, J.-H. He, B. M. Wells, V. A. Podolskiy, J.-K. Wang, *Nano Lett.* **2014**, *14*, 4971.
[32] P. R. Evans, G. A. Wurtz, R. Atkinson, W. Hendren, D. O'Connor, W. Dickson, R. J. Pollard, A. V. Zayats, *J. Phys. Chem. C* **2007**, *111*, 12522.